

Closed Loop Molecular Communication Testbed: Setup, Interference Analysis, and Experimental Results

Lukas Brand, Maike Scherer, Teena tom Dieck, Sebastian Lotter,
Maximilian Schäfer, Andreas Burkovski, Heinrich Sticht, Kathrin Castiglione, and Robert Schober
Friedrich-Alexander-Universität Erlangen-Nürnberg, Erlangen, Germany

Abstract—In this paper, we present a fluid-based experimental molecular communication (MC) testbed that, similar to the human cardiovascular system, operates in a closed circuit pipe system. The proposed system is designed to be biocompatible, resource-efficient, and controllable from outside the pipe. As signaling molecule the testbed employs the *green fluorescent protein variant "Dreiklang"* (GFPD). GFPDs can be reversibly switched via light of different wavelengths between a bright fluorescent state and a less fluorescent state. Hence, this property allows for writing and erasing information encoded in the state of the GFPDs already existing in the fluid via radiation from outside the pipe. The concept of modulating the GFPDs existing in the channel at the transmitter for information transmission instead of releasing new molecules is a form of *media modulation*. In our testbed, due to the closed loop setup and the long experiment durations of up to 250 min, we observe new forms of inter-symbol interferences (ISI), which do not occur in short experiments and open loop systems. In particular, four different forms of inter-symbol interference (ISI), namely channel ISI, inter-loop ISI, offset ISI, and permanent ISI, can occur in the considered system. To mitigate inter-loop ISI and offset ISI, we propose a powerful light based eraser. Finally, we experimentally demonstrate the reliability of information transmission in our testbed achieving error-free transmission of 500 bit at a data rate of 6 bit/min, while employing a sub-optimal low-complexity detection scheme.

I. INTRODUCTION

Synthetic molecular communication (MC) refers to information transmission based on signaling molecules [1]. This paradigm makes it possible to design systems capable of operating in environments unsuitable for electromagnetic wave-based communication, such as the human cardiovascular system. For the latter, the Internet of Bio-Nano-Things (IoBNT) has been proposed, a communication network potentially integrating many in-body nanodevices using MC to exchange information [2].

So far, such systems exist only in theory, i.e., eHealth products and applications based on MC do not exist, yet. To drive research towards first applications, several MC testbeds have been developed in recent years, cf. [3], [4] for a comprehensive overview of existing testbeds. For example, the authors in [5] propose a 2×2 fluid-based multiple-input multiple-output (MIMO) system as a prototype for the IoBNT.

However, the prototype in [5] and all other fluid-based MC testbeds operating in pipes, except that in [6], are open loop. Open loop refers to systems where the ends of the tubes are not connected. As a result, the signaling molecules are added to the pipe system at one end, used *once* to transmit information, and then collected as waste at the other end. There are two major drawbacks to such systems: First, long-term transmission experiments generate a lot of waste. Second, many of the intended applications occur in a closed loop environment, e.g.,

the human cardiovascular system, and cannot be accurately simulated with open loop testbeds.

Therefore, experimental MC system have to be developed that can operate in a closed loop. Currently, there is only one MC testbed that features a closed loop [6]. In [6], a fluid is pumped in a loop system while fluorescent particles are injected, detected, and then diluted. Hence, the applicability of the testbed in [6] for long experiment durations is limited because the signaling molecules can be used only once, which is not resource efficient.

In this context, we propose the first experimental closed loop MC system in which reversibly switchable signaling molecules are reused multiple times, enabled by molecular *media modulation* [7], [8]. In media modulation, the state of signaling molecules already present in the *medium* is changed to transmit information, i.e., no molecules are injected during operation. As signaling molecule, we adopt the biocompatible *green fluorescent protein variant "Dreiklang"* (GFPD) [9], [10]. GFPD molecules can be reversibly switched between a bright fluorescent ON state and a less fluorescent OFF state via light stimuli of mutually different wavelengths [10]. This allows for writing and erasing information employing an optical transmitter (TX) and eraser (EX) in our testbed, respectively. The state of the GFPDs is read out via fluorescence detection at the receiver (RX).

The main contributions of this paper are as follows:

- We utilize media modulation to transmit information in a closed loop pipe system using the states of GFPD molecules. Media modulation enables to locate TX, EX, and RX outside of the pipe. As a result, they do not interfere with the propagation of signaling molecules within the pipe, which is needed, e.g., for healthcare applications.
- Because of the closed loop and long experimental durations, the system is affected by various forms of inter-symbol interference (ISI), some of which have not yet been discussed in the literature before, as they do not occur in open loop systems. These forms of ISI appear on different time scales and are characterized in this work. Furthermore, we discuss and experimentally implement suitable ISI mitigation methods. Moreover, we implement two different detection schemes and test their robustness to ISI.
- We experimentally prove that error-free information transmission of 500 bit at 6 bit min^{-1} and at 2 bit min^{-1} is feasible in a closed loop pipe system. The corresponding experiments take 83 min and 250 min, respectively, during which 9 mL of GFPD solution is permanently reused.

A preliminary and simplified version of the testbed was briefly presented as part of [8]. In [8], the experiment duration was only 3 min, which did not allow to i) evaluate the resource efficiency of the testbed, ii) characterize the ISI, and iii) experimentally determine the symbol error rate (SER) for different detection schemes, which are new contributions of this work.

The remainder of this paper is organized as follows. In Section II and Section III, we describe GFPD and the experimental MC setup, respectively. In Section IV, we characterize the testbed and the different forms of ISI. The employed detection methods are introduced in Section V, and in Section VI, we evaluate the end-to-end communication performance. Finally, Section VII concludes the paper and outlines topics for future work.

II. SIGNALING MOLECULE: GFPD AND ITS PROPERTIES

GFPD is a *photoswitchable* and *biocompatible* green fluorescent protein (GFP) introduced in [10]. In the following, we discuss these two key properties for a MC system.

A. Photoswitchability

In general, photoswitchability of a molecule allows to change its properties upon light exposure of specific wavelengths. In the case of GFPD, photoswitchability allows for a reversible switching of its fluorescence between two¹ distinct states, namely the ON and OFF state, which can be controlled by irradiation of light of different wavelengths. In particular, GFPD may be switched to the ON and OFF states upon irradiation with light of wavelengths $\lambda_{\text{ON}} = 365 \text{ nm}$ and $\lambda_{\text{OFF}} = 405 \text{ nm}$, respectively. The success of the switching depends on the intensity of the irradiation. Furthermore, GFPD can also spontaneously switch back to the ON state due to thermal relaxation. The thermal relaxation of GFPD to the ON state has a half-life of $T_{1/2} = 600 \text{ s}$ at room temperature [10]. Only GFPD in the ON state shows a high fluorescence, i.e., it emits light at a wavelength of $\lambda_E = 529 \text{ nm}$ after being excited by light of wavelength $\lambda_T = 500 \text{ nm}$. Upon repeated photoswitching cycles, photobleaching of GFPD may occur [10]. Here, photobleaching refers to the chemical modification of the GFPD upon strong energy exposure by light. This entails a gradual diminishing of the fluorescence intensity upon repeated irradiation and can be interpreted as GFPD degradation. The authors in [10] show that, for GFPD, the switching efficiency, robustness towards photobleaching, and fluorescence intensity is high, which makes GFPD well suited for the use in our testbed.

B. Biocompatibility

As all GFPs, GFPD is biocompatible [9]. This property allows the use of GFP-based proteins in a wide range of living organisms without causing significant harm or disruption to their normal functions [9]. Thus, the biocompatibility makes GFPDs suitable for *in vivo* usage.

¹In fact, a third state exists, which we denote as *equilibrium state*. In the absence of light, GFPD may switch to this state, which shows a similar fluorescence as the ON state. As the equilibrium state's fluorescence is only slightly higher, in this work, for simplicity of presentation, we do not differentiate between ON state and equilibrium state.

Table I
DEFAULT VALUES FOR EXPERIMENT.

Parameter	Description	Value	Ref.
Testbed Setup			
r_T	Tube radius	$8 \times 10^{-4} \text{ m}$	[11]
L_T	Tube length	2.7 m	
V_T	Tube volume	$\pi r_T^2 L_T = 5.43 \text{ mL}$	
V_R	Reservoir volume	2.50 mL	
V_{PF}	Volume of pump and flow cell	1.07 mL	
V_S	Total volume of system	$V_S = V_{PF} + V_R + V_T = 9.00 \text{ mL}$	
Q	Volume flux	9.45 mL min^{-1}	
v_{eff}	Effective flow velocity	0.078 m s^{-1}	
T_L	Average loop duration	41 s	
$L_{\text{EX}} \& L_{\text{TX}}$	EX & TX length	0.29 m	
L_{RX}	RX length	$3 \times 10^{-3} \text{ m}$	
$d_{\text{TX,RX}}$	Distances between end of TX and start of RX	0.06 m, 0.63 m	
T_I	Irradiation duration	10 s	
T_G	Guard interval	0 s, 20 s	
T_S	Symbol duration	10 s, 30 s	
Δt	Sampling time step	2 s	
GFPD Specific Parameter			
C_{GFPD}	Concentration of GFPD	0.3 mg mL^{-1}	
M_{GFPD}	Molar mass	26900 g mol^{-1}	[10]
λ_{OFF}	Wavelength for switching OFF ^(a) / ON ^(b)	405 nm / 365 nm	[10]
λ_T	Wavelength for fluorescence excitation ^(c)	500 nm	[10]
λ_E	Fluorescence emitting wavelength	529 nm	[10]
$T_{1/2}$	Half time in OFF state	600 s	[10]

(a) Used at TX.
(b) Used at EX.
(c) Used at RX.

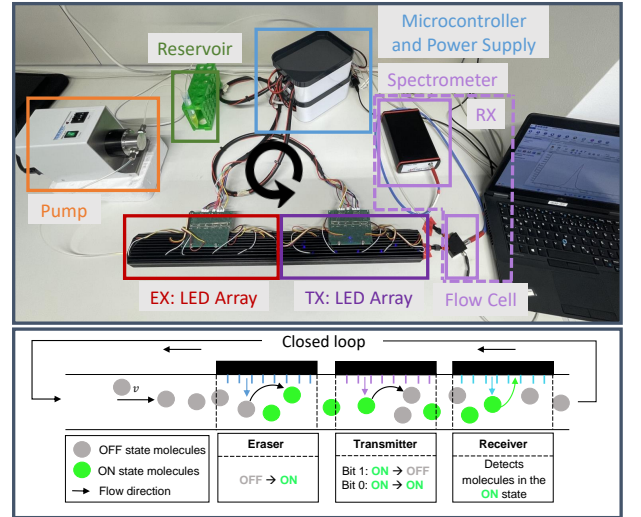


Figure 1. Top: Overview of the building blocks of the experimental closed loop MC setup using GFPD as signaling molecule. The setup comprises a reservoir, a pump, connecting tubes, LED arrays for EX and TX, and the RX which consists of an LED connected to a fluorescence flow cell and a spectrometer. The LED arrays are controlled via a microcontroller and are supplied with power by cable. Bottom: Schematic representation of the pipe containing GFPD dissolved in fluid. The GFPDs can be switched to the OFF state and to the ON state by the EX and TX, respectively, while the state of GFPD can be determined at the RX.

III. TESTBED SETUP

In this section, we introduce the testbed. Fig. 1 shows the entire testbed (top panel) as well as a schematic representation of its working principle (bottom panel). Moreover, we highlight the different building blocks of the testbed by colored boxes in Fig. 1. If not noted otherwise, the default parameter values used in our experiments are given in Table I.

A. Experiment Preparation

1) *GFPD Solution*: In all experiments, we use $V_S = 9 \text{ mL}$ of GFPD solution. The GFPD solution is composed of a buffer solution with GFPDs of a concentration of $C_{\text{GFPD}} = 0.3 \text{ mg mL}^{-1}$ uniformly dissolved in the buffer.

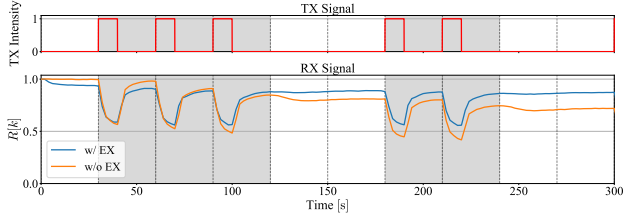


Figure 2. Setting: $T_I = 10$ s, $T_G = 20$ s. Transmission of a bit sequence using the normalised TX intensity (red). The received fluorescence intensity of the system at $\lambda_E = 529$ nm with (blue) and without (orange) the use of an EX, respectively. The gray shaded symbol intervals highlight bit 1 transmissions.

2) *Pipe System, Reservoir, and Pump*: As the first step in all experiments, we fill the pipe, the reservoir, and the segments within the pump and the flow cell with $V_T = 5.43$ mL, $V_R = 2.50$ mL, and $V_{PF} = 1.07$ mL of the GFPD solution, respectively. As pipe we use a fluorinated ethylene propylene (FEP) tube with radius $r_T = 8 \times 10^{-4}$ m and total length $L_T = 2.7$ m. The reservoir is realized by a falcon tube and needed in our system to close the circuit, i.e., both ends of the tube are immersed in the fluid within the reservoir and are hereby connected. During operation, the GFPD solution is pumped through the tube and the reservoir using a gear pump generating an effective volume flux of $Q = 9.45$ mL min $^{-1}$, which results in $v_{\text{eff}} = 0.078$ m s $^{-1}$ for the given tube radius. Hence, the average duration T_L , that one GFPD molecule needs to circulate one time through the testbed, can be approximated as $T_L = \frac{V_{PF} + V_T}{Q} = 41$ s, assuming, on average, no duration of stay in the reservoir.

B. Information Transmission

While the pump transports the GFPDs within the circuit as described above, information can be modulated from outside the pipe into the state of the GFPDs by an LED based TX. Later the RX reads out the state of the GFPD via fluorescence triggered by an LED. Additionally, an LED based EX can be used to erase the modulated information. This modulation method is referred to as media modulation and schematically represented in the bottom part of Fig. 1.

The LEDs of the TX, EX, and RX are controlled by an ESP32-S2 microcontroller. In the following, the practical realization and use of TX, RX, and EX are presented in detail. Additionally, we show measurements to support the understanding of the function of the three components.

1) *Transmitter*: The TX is used to modulate binary information via media modulation into the state of the GFPDs. The TX comprises an LED array with 12 equally spaced LEDs which can emit light at a wavelength of $\lambda_{\text{OFF}} = 405$ nm. The LED array is attached to an aluminium circuit board. The board has a total length of $L_{\text{TX}} = 29$ cm and is fixed to a passive cooling element to increase the LED operation life time. Moreover, the LEDs are individually wired to guarantee maximum flexibility of our testbed. In the long run, this allows the individual control of each LED during the experiments. However, in this work, all LEDs are used simultaneously.

To transmit information, for bit 1, the TX irradiates with maximum intensity for an irradiation duration of T_I to trigger the switching to the OFF state of the available GFPD molecules, i.e., molecules which are below the TX module during irradiation. For a bit 0, the TX is off during T_I . T_I is followed by

a guard interval of duration T_G , during which the TX is always inactive. This results in a symbol duration of $T_S = T_I + T_G$.

The top panel of Fig. 2 shows the normalised TX intensity (red line) as a function of time, which is used to transmit the exemplary bit sequence $\langle 0, 1, 1, 1, 0, 0, 1, 1, 0, 0 \rangle$ with $T_I = 10$ s, $T_G = 20$ s, from which $T_S = 30$ s follows. In Fig. 2, bit 1 transmissions are shaded in gray. For all our experiments in this paper, we use $T_I = 10$ s. As guard intervals, $T_G = 0$ s and $T_G = 20$ s are considered, which results in $T_S = 10$ s and $T_S = 30$ s, respectively.

2) *Receiver*: The RX is used to read out the current state of the GFPD. The RX is placed at a distance of $d_{\text{TX,RX}}$ after the end of the TX. If not noted otherwise, we use $d_{\text{TX,RX}} = 0.06$ m. The RX is comprised of a fluorescence flow cell (FIA-SMA-FL-ULT - Ocean Optics) equipped with a $\lambda_T = 500$ nm LED used to trigger the fluorescence of GFPD. The emitted light upon fluorescence is guided by an optical fiber to a spectrometer (Avantes), where the fluorescence intensity is recorded using AvaSoft 8. We denote the received signal after isolating the part of the signal close to the wavelength of interest, i.e., $\lambda_E = 529$ nm, as $R[k]$. $R[k]$ provides the fluorescence intensity at time instances $t_k = k\Delta t$ with $k = 0, 1, 2, \dots, k_{\text{max}}$, where Δt denotes the time difference between two samples. $k_{\text{max}} = \frac{T_{\text{rec}}}{\Delta t}$ depends on the absolute time length T_{rec} of the signal recorded by the spectrometer. In this work, we use $\Delta t = 2$ s if not noted otherwise.

The bottom panel of Fig. 2 shows the measured $R[k]$ (orange line) as a function of time in response to the TX irradiation intensity. Note that in this case no EX is used, which is indicated by the label w/o EX. $R[k]$, as expected, shows clear fluorescence intensity drops for bit 1. Conversely, during a bit 0 transmission, the received fluorescence intensity signal shows no drop and remains at a high fluorescence intensity level. Note that we can already see here that the exact shape of $R[k]$ for the current bit depends on the previously sent bits, indicating the existence of ISI, which is discussed in detail in Section IV-C.

3) *Eraser*: The EX can be used to reset the state of the GFPD molecules to the ON state. The EX component comprises an LED array with 12 equally spaced LEDs operating at $\lambda_{\text{ON}} = 365$ nm and has a total length of $L_{\text{EX}} = 29$ cm. It is placed upstream next to the TX. When we use the EX in an experiment, the EX is continuously active. Hereby, it enables the switching of the GFPDs from the OFF state back to the ON state. Hence, with an EX the number of available ON state molecules at the TX is increased.

Fig. 2 shows the measured $R[k]$ as a function of time with an active EX (blue line), which is labeled as w/ EX. We observe that still clear peaks are visible in $R[k]$ for bit 1 transmission. However, with the EX, the received signal for bit 0 transmissions is almost constant, which is desired².

IV. COMMUNICATION LINK CHARACTERIZATION

In this section, we mathematically model the received signal and characterize the different forms of ISI present in the testbed.

²In fact, for the first bit 0, Fig. 2 shows a slight drop of $R[k]$ which is not observed for experiments without the EX. We explain the drop with the EX with the switching of the GFPD molecules from the equilibrium state, cf. Footnote 1 in Section II-A, to the slightly less fluorescent ON state in the beginning of the experiment.

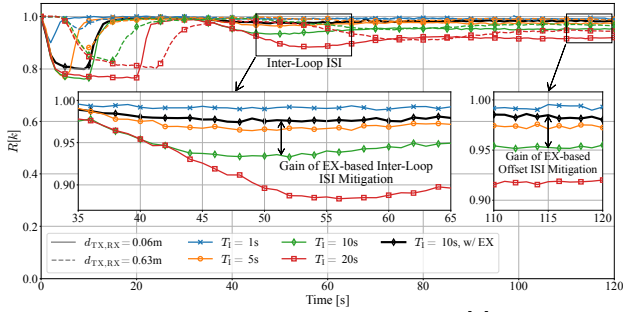


Figure 3. Recorded fluorescence intensity signal $R[k]$ as a function of time for different irradiation durations T_1 and TX-RX distances $d_{TX,RX} = 0.06$ m and $d_{TX,RX} = 0.63$ m. Here, we use $\Delta t = 1$ s.

A. Mathematical Description of the Received Signal and the Pilot Sequence

In the investigated experimental MC system, N_{Sym} binary symbols $b[i]$ with $b \in \{0, 1\}$, $i = 0, 1, 2, \dots, N_{\text{Sym}} - 1$ are transmitted and signal $R[k]$ is received. $R[k]$ can be subdivided into parts as follows

$$\mathcal{R}_i[k] = R \left[k + i \frac{T_S}{\Delta t} \right] \quad \text{for } 0 \leq k < \frac{T_S}{\Delta t}, \quad (1)$$

where signal $\mathcal{R}_i[k]$ corresponds to symbol i . For detection, we use samples $d[i] = \mathcal{R}_i[k_p]$, i.e., we use one sample $d[i]$ per symbol i , which corresponds to the sample instant k_p , where the local minimum for bit 1 transmission is expected. The value of k_p is experimentally determined based on a pilot sequence b^P of length L_P , i.e., given by $b[i]$, $i \in \{0, 1, \dots, L_P - 1\}$, which is sent at the beginning of each transmission and is known at the RX. In particular, to obtain k_p , we take the median of the sample instants of the local minima of all bit 1 transmissions in b^P . For the experiments shown in this work, we use the pilot sequence $b^P = b[i] = \langle 0, 1, 1, 1, 0, 0, 1, 1, 0, 0 \rangle$, $i \in \{0, 1, \dots, 9\}$, of length $L_P = 10$, which is identical to the bit sequence shown in Fig. 1.

B. Signal Impulse Responses

Fig. 3 shows the received signals for different TX and channel settings for a single bit 1 transmission. In particular, we vary the TX irradiation duration T_1 and $d_{TX,RX}$. Increasing T_1 also increases the fluorescence intensity drop until for $T_1 = 5$ s and $T_1 = 10$ s the signal exhibits a floor for $d_{TX,RX} = 0.06$ m and $d_{TX,RX} = 0.63$ m, respectively. Increasing T_1 further does not change the fluorescence intensity as the average energy that a GFPD molecule receives is limited. In particular, the average energy received by a GFPD is dependent on the irradiation power P of the LEDs at the TX, the average flow velocity v_{eff} , the length of the TX L_{TX} , and T_1 . A detailed investigation of this aspect is left for future work.

Moreover, we see in Fig. 3 that increasing $d_{TX,RX}$ from $d_{TX,RX} = 0.06$ m to $d_{TX,RX} = 0.63$ m results in a less severe fluorescence intensity drop, as the modulated GFPDs have more time to spontaneously switch back to the ON state and disperse further during the propagation from TX to RX. The different forms of ISI, which are visible in Fig. 3, are discussed in the next section.

C. ISI Characterization and Mitigation

We identified four different forms of ISI in our testbed, with three of them appearing only for long experiments in closed

loop systems. These forms of ISI occur on different time scales and are discussed in the following.

1) *Channel ISI*: During their propagation within the channel from TX to RX, signaling molecules from consecutive symbols may overlap, leading to ISI. To differentiate between different forms of ISI, we further specify this form as *channel ISI*. Channel ISI has been observed in existing MC testbeds, e.g., [12], [13]. We refer to [13] for a comprehensive discussion of channel ISI.

Channel ISI can be mitigated by using a guard interval, during which the TX is inactive and the signaling molecules have time to be carried out of the channel before the next symbol is transmitted. Of course, the success of the mitigation depends on the guard interval duration T_G , and improves for increasing T_G . However, increasing T_G decreases the data rate, i.e., there exists a tradeoff between channel ISI intensity and data rate. Note that also without a guard interval, the effect of channel ISI (and not channel ISI itself) may vary dependent on the symbol duration T_S and when $\mathcal{R}_i[k]$ is sampled to obtain $d[i]$.

2) *Inter-Loop ISI*: Due to the closed loop, a second form of ISI occurs, which we call *inter-loop ISI*. As the signaling molecules remain in the system, they may interfere not only with neighbouring symbols but also with symbols transmitted much later. In particular, GFPD molecules, which are switched to the OFF state during a bit 1 transmission, may propagate several circles in the loop before they spontaneously switch back to the ON state. Hereby, these signaling molecules likely impact the received signal multiple times, while the distinctness and the number of recurrences depend on the length of the loop and the half time of the OFF state $T_{1/2}$. Inter-loop ISI is visible as a dip in the received signal, cf. Fig. 3, and can be reduced by utilizing an EX. Note that the first inter-loop ISI peak appears approximately 35 s after the main peak, which is close to the calculated loop duration of T_L . Furthermore, Fig. 3 shows that inter-loop ISI becomes increasingly severe as T_1 increases.

3) *Offset ISI*: We observe that part of the received dips, referred to as inter-loop ISI, are eventually transformed to a fluorescence intensity floor with an overall lower fluorescence intensity level compared to the initial fluorescence intensity level. This happens as the signaling molecules causing the inter-loop ISI disperse within the system. We refer to this form of ISI as *offset ISI*. In consequence, for strong offset ISI, the received fluorescence intensity in response to a bit 0 transmission is reduced, and therefore closer to the intensity in response to a bit 1 transmission. This affects the reception performance. The intensity of offset ISI depends on the number of bit 1 transmissions, T_1 , and $T_{1/2}$, and can be mitigated by using an EX. The right inset of Fig. 3 shows that offset ISI increases for increasing T_1 , visible as the increasing difference between $R[k]$ and the initial fluorescence intensity.

4) *Photobleaching and Permanent ISI*: Finally, upon extensive irradiation, GFPD molecules may be permanently degraded. This effect occurs in long experiments and is referred to as photobleaching. While the decrease in fluorescence intensity due to offset ISI is reversible, photobleaching results in a long term and permanent decrease of GFPD fluorescence. As GFPD is irradiated by the EX, the RX, and the TX in the

testbed, all three light sources contribute to photobleaching. Therefore, we denote the components caused by the TX, by the EX, and by the RX as *permanent ISI*, *eraser bleaching*, and *measurement bleaching*, respectively³. Photobleaching affects the availability of GFPD for media modulation and hereby impacts the transmission of future symbols. Photobleaching is increased by increasing the irradiation energy, e.g., by increasing the irradiation power or increasing the irradiation duration [10, Suppl. Fig. 7]. Therefore, there exists a tradeoff in switching accuracy, which increases for increasing irradiation energy provided by the EX and TX, and photobleaching. We observe that photobleaching limits the maximum duration of our experiments. As it manifests itself only after many transmission cycles, it is not visible in Fig. 3.

5) *ISI Mitigation*: To overcome inter-loop and offset ISI, we exploit the spontaneous switching property of GFPD and the EX for passive and active inter-loop and offset ISI mitigation, respectively. In fact, GFPD can spontaneously switch back from the OFF state to the ON state with a half-life of $T_{1/2} = 600$ s. Hereby, information modulated to the state of the GFPD is erased naturally, and offset ISI is reduced. In addition, the EX actively triggers the switching to the ON state. If the EX is ideal, it switches all traversing GFPDs from the less fluorescent OFF state to the fluorescent ON state. Of course, in reality, only a fraction of the GFPD may be switched because the power of the LED is limited. Fig. 3 reveals the success of EX based ISI mitigation for $T_1 = 10$ s. In particular, we see that both inter-loop ISI and offset ISI are reduced, which increases the overall fluorescence intensity by approximately 4%⁴.

V. DETECTION METHOD

In the following, we describe two different threshold detection schemes. In all cases, the pilot sequence b^P is used to determine the optimal threshold value. However, the detection techniques differ in terms of complexity. The basic threshold detection (BD), presented in Section V-A, uses symbol-by-symbol detection, i.e., each symbol is detected independent of the other symbols. In contrast, the differential threshold detection (DD) introduced in Section V-B exploits two consecutive samples.

A. Basic Threshold Detector

For the BD, the threshold ξ_R is used to estimate the transmitted symbol as follows

$$\hat{b}_R[i] = \begin{cases} 0, & \text{if } d[i] \geq \xi_R \\ 1, & \text{otherwise} \end{cases}. \quad (2)$$

To find a suitable threshold, we choose the threshold value ξ_R that minimizes the Hamming distance between the symbols of pilot sequence b^P and its estimate. If the choice of ξ_R is ambiguous, i.e., more than one ξ_R minimizes the Hamming distance, we select the lowest of the possible values. Once ξ_R is computed from the pilot sequence, the symbols $\hat{b}_R[i]$ for $i \in \{L_P, \dots, N_{\text{Sym}} - 1\}$ are estimated based on (2).

³Note that only the TX irradiation varies as a function of the transmit sequence. Therefore, only the photobleaching caused by the TX can be denoted as ISI, whereas the photobleaching caused by the EX and the RX is independent of the transmission sequence.

⁴Note that the forms of ISI mitigation described here impact the signaling molecules themselves. Hence, unlike equalization schemes, they are not part of the detection scheme at the RX and therefore do not contribute to the computational complexity needed for detection.

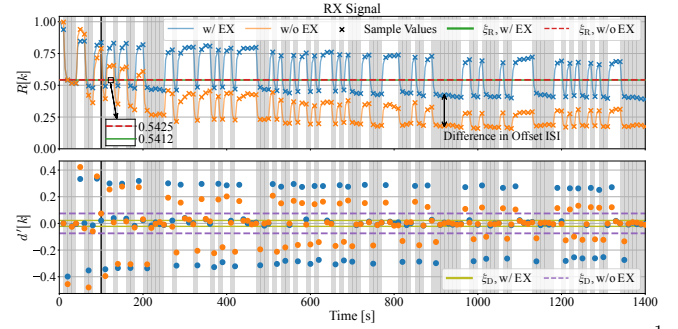


Figure 4. Setting: $T_1 = 10$ s, $T_G = 0$ s, from which $R = 6.0$ bit min^{-1} follows. (Top): Recorded signal and BD. The first segment of the received fluorescence intensity of a 84 min long experiment and the basic threshold values ξ_R as defined in Section V-A as a function of time, respectively. The markers indicate the sampled values used for detection. (Bottom): DD scheme. The differentiated samples (dots) and the differential threshold values ξ_D as defined in (6) as a function of time. General: The gray shaded symbol intervals highlight bit 1 transmissions. The vertical line (solid black) indicates the end of the pilot sequence considered to derive the threshold values.

B. Differential Threshold Detector

Another threshold based approach is the DD scheme. The DD has been proposed for MC in [14] and implemented for an MC testbed in [12]. In fact, in [12], the authors have shown the robustness of the DD scheme against a slow drift in the received signal, which motivates the usage of such a detector also in this work.

For DD, the difference $d'[i]$ between the current sample and the sample of the previous symbol is utilized. $d'[i]$ is defined as follows

$$d'[i] = \begin{cases} 0, & \text{for } i = 0 \\ d[i] - d[i-1], & \text{otherwise} \end{cases}. \quad (3)$$

If the preceding and the current symbol are equal, the difference between the sampling values, i.e., $d'[i]$ is presumably small in its absolute value. If a change in transmitted symbols occurs, then $d'[i]$ will have a larger absolute value. In this case, if a bit 0 is transmitted after a bit 1, we expect $d'[i] > 0$ and if a bit 1 follows a bit 0, $d'[i] < 0$. These considerations are exploited in the decision rule of this DD as follows

$$\hat{b}_D[i] = \begin{cases} \hat{b}_D[i-1], & \text{if } |d'[i]| \leq \xi_D \\ \frac{1 - \frac{d'[i]}{|d'[i]|}}{2}, & \text{otherwise} \end{cases}. \quad (4)$$

To find a suitable value for ξ_D , we first determine the set of indices of transmitted pilot symbols that are a repetition of its preceding symbol as follows

$$\mathcal{K}_P^P = \{i \mid b[i] = b[i-1], i \in \{0, 1, \dots, L_P - 1\}\}. \quad (5)$$

Then, we use this set to find the threshold ξ_D as follows

$$\xi_D = \max_{i \in \mathcal{K}_P^P} |d'[i]|. \quad (6)$$

VI. END-TO-END COMMUNICATION PERFORMANCE

In this section, we discuss the end-to-end communication performance of the developed testbed. In particular, we evaluate the SER for different transmission lengths N_{Sym} and different data rates R using the detection schemes discussed in Section V. We show results with and without EX-based ISI mitigation.

A. Visualizing the Detection Schemes

The top of Fig. 4 shows the normalized fluorescence intensity (solid orange and blue lines) over time and the sampled values $d[i]$ (markers) using as setting $T_1 = 10$ s and $T_G = 0$ s.

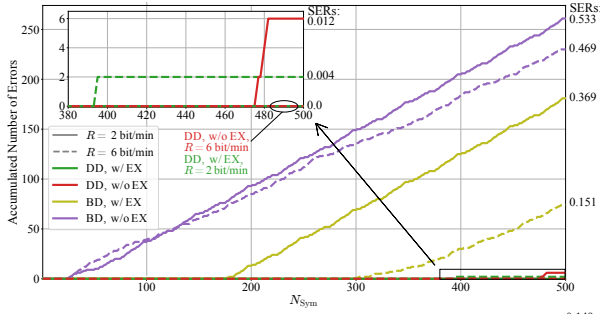


Figure 5. Detection accuracy: Accumulated number of transmission errors as a function of the transmission sequence length N_{Sym} for different data rates and detection schemes. Data rates of $R = 2.0 \text{ bit min}^{-1}$ and $R = 6.0 \text{ bit min}^{-1}$ are achieved with $T_I = 10 \text{ s}$, $T_G = 20 \text{ s}$, cf. Fig. 2, and $T_I = 10 \text{ s}$, $T_G = 0 \text{ s}$, cf. Fig. 4, respectively. w/ EX and w/o EX indicate the cases with and without EX based ISI mitigation, respectively.

In addition, the bottom of Fig. 4 shows the corresponding difference of two consecutive samples $d'[i]$ (dots). We further show the threshold values ξ_R and ξ_D , which are derived based on the pilot sequence, whose end is highlighted by a black vertical solid line.

Fig. 4 shows that even without a guard interval clear peaks are visible in the received signal for bit 1 transmissions. We observe that the amplitude of the recorded signals $R[k]$ decreases over time, which is expected. In fact, without the EX, the overall fluorescence intensity level decreases fast, which is due to increasing offset ISI, cf. Section IV-C. In contrast, when using the EX, the decrease is slower, however still existing. We conclude that in this case the decrease is mainly caused by degradation of GFPD due to photobleaching, cf. Section II. Moreover, we observe from the bottom panel that the dots, which denote $d'[k]$, are closer to $d' = 0$ over time. This indicates that the difference of the fluorescence intensity levels of bits 0 and bits 1 decreases over time, posing a challenge especially for long experiments.

Fig. 4 further shows that ξ_R is identical for the cases with and without EX and is, in this case, determined by the second sample within the pilot sequence of length $L_P = 10$. In fact, the second sample appears at a time instant where $R[k]$ has not yet been impacted by the EX, which explains the similarity. Moreover, we observe that ξ_D used for the case without EX is larger compared to that for the case with EX. This is intuitive as $R[k]$ for the EX-free case varies more, which is reflected in the larger ξ_D . Note that a larger difference for ξ_R and ξ_D between the cases with and without EX is expected when increasing L_P or when reducing the loop duration T_L .

B. SER Evaluation

Fig. 5 shows the accumulated number of transmission errors as a function of the transmission sequence length N_{Sym} for different settings. Hence, in this plot, horizontal lines indicate error free transmission for the length of the line. Additionally, we show the SER for $N_{\text{Sym}} = 500$, which is the largest number of symbols transmitted.

First, we concentrate on the results for $R = 6.0 \text{ bit min}^{-1}$. From Fig. 5, we observe that the BD scheme enables error-free MC only at the beginning of the experiment. For long transmissions, the BD scheme yields a poor performance compared to the DD scheme based on ξ_D . In fact, due to offset ISI and photobleaching, the channel state information

gained by the pilot sequence and used for the computation of ξ_R is eventually outdated, which leads to an increase in errors. This can also be observed in top panel of Fig. 4, where for $t > 200$ the entire orange curve is below ξ_R . We observe that when using an EX to mitigate offset ISI the first errors occur later. We observe that the DD, due to its robustness to channel state uncertainties, causes only two symbol errors and freedom from errors for the cases with and without EX, respectively. In particular, offset ISI and photobleaching effects are successfully canceled out when taking the difference between two consecutive samples. We conclude that when using the DD, there exist system settings, where an EX is not essential.

Finally, we observe that decreasing the data rate from $R = 6.0 \text{ bit min}^{-1}$ to $R = 2.0 \text{ bit min}^{-1}$ by using a guard interval of duration $T_G = 10 \text{ s}$ increases the error rate, which seems counter intuitive at first. In fact, using $T_G = 10 \text{ s}$ is expected to decrease the impact of channel ISI, while leaving the other forms of ISI unmodified. However, as for $R = 2.0 \text{ bit min}^{-1}$ the experiment takes three times as long, eraser bleaching and measurement bleaching is increased, which explain the performance loss.

VII. CONCLUSION

In this work, we introduced our experimental closed loop pipe-based testbed, which can be used for MC using GFPD as signaling molecule. We showed that media modulation can successfully encode binary digital data through an optical signal into a molecular signal, which then can be detected at the RX, enabling reliable MC. We identified and characterized inter-loop ISI, offset ISI, and permanent ISI as new forms of ISI, which occur for long experiments in self-contained setups and appear on different time scales. Finally, we proved that our testbed enables error-free signal transmission of 500 bit at a data rate of 6.0 bit min^{-1} when using a DD.

While, in this work, we identified new forms of ISI and proposed methods to mitigate them, it would be helpful to understand, how to handle possible resulting tradeoffs. For example, analyzing the tradeoff between EX based ISI mitigation and eraser bleaching, which limits the operation duration of the testbed, is an interesting topic left for future work. In addition, investigating the potential of increasing the data rate by using higher-order modulation via different irradiation intensities seems promising.

REFERENCES

- [1] T. Nakano, A. W. Eckford, and T. Haraguchi, *Molecular communication*. Cambridge, U.K.: Cambridge Univ. Press, Sep. 2013.
- [2] I. F. Akyildiz, M. Pierobon, S. Balasubramaniam, and Y. Koucheryavy, "The internet of bio-nano things," *IEEE Commun. Mag.*, vol. 53, no. 3, pp. 32–40, 2015.
- [3] S. Lotter *et al.*, "Experimental research in synthetic molecular communications – Part I," *IEEE Nanotechnol. Mag.*, vol. 17, no. 3, pp. 42–53, Jun. 2023.
- [4] —, "Experimental research in synthetic molecular communications – Part II," *IEEE Nanotechnol. Mag.*, vol. 17, no. 3, pp. 54–65, Jun. 2023.
- [5] C. Lee, B.-H. Koo, C.-B. Chae, and R. Schober, "The internet of bio-nano things in blood vessels: System design and prototypes," *J. Commun. Netw.*, Apr. 2023.
- [6] N. Tuccitto, G. Li-Destri, G. M. Messina, and G. Marletta, "Fluorescent quantum dots make feasible long-range transmission of molecular bits," *J. Phys. Chem. Lett.*, vol. 8, no. 16, pp. 3861–3866, Aug. 2017.
- [7] L. Brand *et al.*, "Media modulation based molecular communication," *IEEE Trans. Commun.*, vol. 70, no. 11, pp. 7207–7223, Sep. 2022.

- [8] —, “Switchable signaling molecules for media modulation: Fundamentals, applications, and research directions,” *IEEE Commun. Mag.*, pp. 1–7, Sep. 2023.
- [9] H. A. Richards, C.-T. Han, R. G. Hopkins, M. L. Failla, W. W. Ward, and C. N. Stewart Jr, “Safety assessment of recombinant green fluorescent protein orally administered to weaned rats,” *J. Nutr.*, vol. 133, no. 6, pp. 1909–1912, Feb. 2003.
- [10] T. Brakemann *et al.*, “A reversibly photoswitchable GFP-like protein with fluorescence excitation decoupled from switching,” *Nat. Biotechnol.*, vol. 29, no. 10, pp. 942–947, Sep. 2011.
- [11] J. E. Hall and M. E. Hall, *Guyton and Hall Textbook of Medical Physiology e-Book*. Philadelphia, PA, USA: Elsevier Health Sciences, 2020, vol. 12th ed.
- [12] L. Grebenstein *et al.*, “Biological optical-to-chemical signal conversion interface: A small-scale modulator for molecular communications,” in *Proc. 5th. Int. Conf. Nanosc. Comp. Commun. (NANOCOM)*, 2018, pp. 1–6.
- [13] J. Wang, D. Hu, C. Shetty, and H. Hassanieh, “Understanding and embracing the complexities of the molecular communication channel in liquids,” in *Proc. 26th Int. Conf. Mob. Comput. Netw. (MOBICOM)*, 2020, pp. 1–15.
- [14] B. Li, M. Sun, S. Wang, W. Guo, and C. Zhao, “Low-complexity noncoherent signal detection for nanoscale molecular communications,” *IEEE Trans. NanoBioscience*, vol. 15, no. 1, pp. 3–10, Dec. 2015.

ACKNOWLEDGMENT

We thank Prof. Stefan Jakobs (Max Planck Institute for Biophysical Chemistry, Göttingen, Germany) for providing a plasmid encoding Dreiklang.